RSC Advances

PAPER

View Article Online
View Journal | View Issue

Cite this: *RSC Adv.*, 2022, **12**, 33516

A promising 1D Cd-based hybrid perovskite-type for white-light emission with high-color-rendering index†

Mahdi Gassara,[a] Rawia Msalmi,[a] Xinghui Liu,[b] Fredj Hassen,[c] Anna Moliterni,[d] Naoufel Ben Hamadi,[e] Ahlem Guesmi,[e] Lotfi Khezami,[e] Taoufik Soltani[f] and Houcine Naïli *[a]

Received 27th July 2022
Accepted 14th November 2022

DOI: 10.1039/d2ra04676h

rsc.li/rsc-advances

A one dimensional (1D) perovskite-type $(C_6H_7NBr)_3[CdBr_5]$ (abbreviated 4-BAPC) was synthesized by slow evaporation at room temperature (RT). 4-BAPC crystalizes in the monoclinic system with the space group $P2_1/c$. The 1D inorganic chains are formed by corner sharing $CdBr_6$ octahedra. Thermal measurement shows that 4-BAPC is stable up to 190 °C. Optical characterization demonstrates that the grown crystal is an indirect bandgap material with a bandgap value of 3.93 eV, which is consistent with theoretical calculations. The electronic structure, calculated using density functional theory, reveals that the valence band originates from a combination of Br-4p orbitals and Cd-4d orbitals, whereas the conduction band originates from the Cd-5s orbitals. The photoluminescence spectroscopy shows that the obtained material exhibits a broad-band white light emission with extra-high CRI of 98 under $\lambda_{exc} = 380$ nm. This emission is mainly resulting from the self-trapped exciton recombinations within the inorganic $CdBr_6$ octahedron, and the fluorescence within the organic conjugated ammonium salt.

Introduction

Nowadays, solid-state lighting technology is very important in our daily life because of its incredible applications for human development.[1–3] To produce white-light in light-emitting diodes (LEDs), three main processes are used. The first process consists of coating a mixture of red, green, and blue (RGB) phosphors in an ultraviolet LED.[4,5] The second process requires using a mixture of RGB LEDs to create WL,[6,7] and the third process consists of coating a yellow phosphor in a blue LED.[8,9] Despite their advantages, each process has its own cons such as low efficiency, low color rendering, and discontinuity in the photoluminescence spectrum.[10–12] Hybrid organic–inorganic perovskite materials (HOIPM) have gained much attention after being reported as semiconductors in 1990.[13–16] After the release of $(CH_3NH_3)[PbI_3]$[17] in 2009 as a high performance semiconductor solar absorber in the first perovskite solar cell with great potential and low cost, HOIPM becomes one of the most important research topics in the field of material chemistry during the past decade. Owing to their wide band gap and low dimensional, HOIPM show an extreme performance in diverse optoelectronic applications such as LEDs,[18–20] lasers[21] and photodetectors.[22] In the last ten years, researchers reported that white light emission was easily observed in two-dimensional HOIPM such as the $(EDBE)[PbBr_4]$,[23] $(N\text{-}MEDA)[PbBr_4]$,[24] $(C_6H_{11}NH_3)_2[PbBr_4]$[25] and $(C_3H_8N_6)[PbBr_4]$.[26] White-light emission occurs when the self-trapping mechanism, resulting from strong electron–phonon coupling, is observed inside a distorted inorganic lattice.[23,27,28] The performance of the white light emitter depends on two critical parameters, the color rendering index (CRI)[29–31] and CIE chromaticity coordinates.[32] The CRI describes the ability of the light source to render the colors of various objects with comparison to the natural sunlight.[12,31] In general, the commercial LEDs show a CRI value about 80 which is considered acceptable for human eye-friendly applications. However, high-level industrial lighting applications, such as cinematography, surgery and museum galleries require an ultra-high CRI greater than 90.[33,34] Previous researches on structure-properties correlation in low-dimensional metal halides structures demonstrated that 1D perovskites with large

[a]*Laboratory Physico Chemistry of the Solid State, Department of Chemistry, Faculty of Sciences of Sfax, Sfax University, Tunisia. E-mail: houcine.naili@fss.rnu.tn; houcine_naili@yahoo.com*

[b]*Department of Chemistry, Sungkyunkwan University (SKKU), 2066 Seoburo, Jangan-Gu, Suwon 16419, Republic of Korea*

[c]*Laboratoire de Micro-Optoélectronique et Nanostructures (LMON), Faculté des Sciences de Monastir, Université de Monastir, Avenue de l'environnement, Monastir, 5019, Tunisia*

[d]*Institute of Crystallography–CNR, Via Amendola, 122/O70126 Bari, Italy*

[e]*Chemistry Department, College of Science, IMSIU (Imam Mohammad Ibn Saud Islamic University), P.O. Box 5701, Riyadh 11432, Saudi Arabia*

[f]*Physics Laboratory of Soft Matter and Electromagnetic Modelling, Faculty of Sciences of Tunis, University of Tunis El Manar, Tunis, Tunisia*

† Electronic supplementary information (ESI) available. CCDC 2092549. For ESI and crystallographic data in CIF or other electronic format see DOI: https://doi.org/10.1039/d2ra04676h

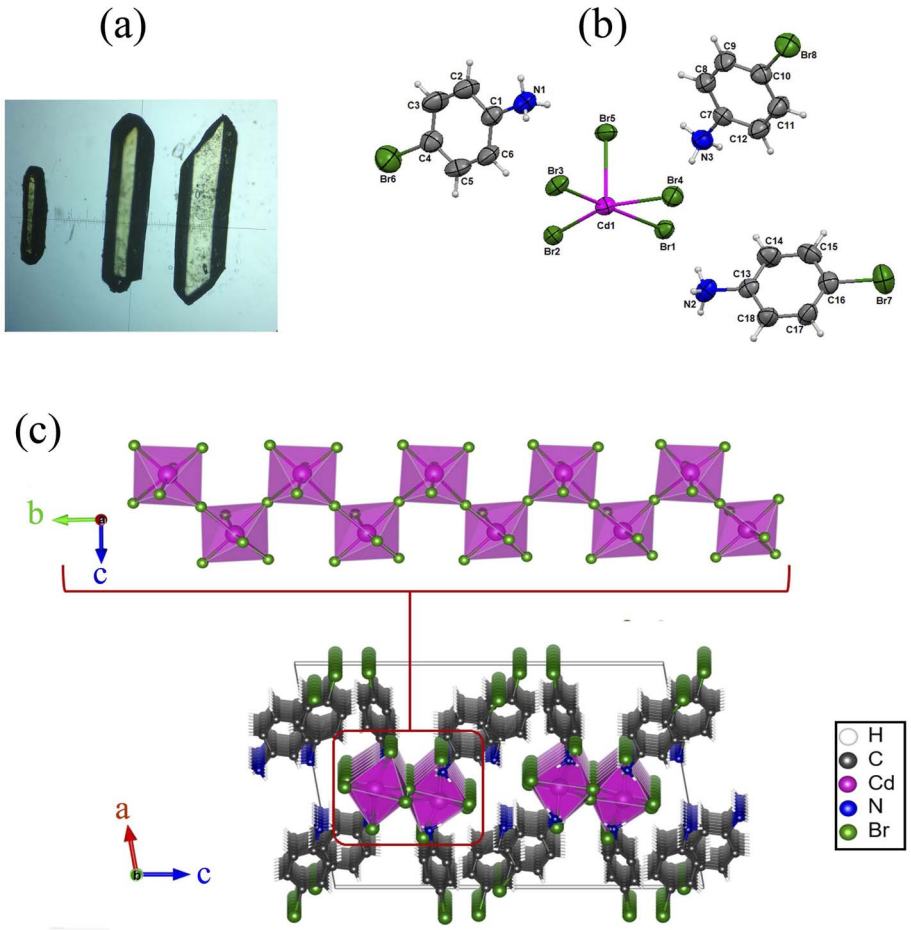

Fig. 1 (a) Optical microscopy image of the microcrystals (×50), (b) asymmetric unit of 4-BAPC, (b) 1D inorganic infinite chain and (c) packing framework 4-BAPC.

band gap could exhibit superior photoluminescence (PL) properties.[35–40] In 1D-hybrid metal halide systems, the 1D assembly of the six coordinated octahedra present in general four different types of connection: face-sharing, edge-sharing, corner-sharing and a mixed connection modes.[41] In this study, we report a new 1D Cd-based hybrid perovskite-type $(C_6H_7NBr)_3[CdBr_5]$. This material demonstrates a high ability to emit a bright white-light with a CIE chromaticity coordinate of (0.30, 0.32), an ultrahigh CRI of 98, and a correlated color temperature (CCT) of 6812 K. The experimental optical analysis and the theoretical calculation, using the density functional theory (DFT), prove that our compound belongs to large gap semiconductors and that it is suitable for optoelectronic applications as white-light emitter.

Experimental section

Synthesis

All chemical products were purchased from Sigma-Aldrich and used without any further purification. An aqueous solution containing $CdBr_2 \cdot 4H_2O$ (1 mmol, 0.34 g), 4-bromoaniline (3 mmol, 0.55 g) and 0.2 ml of hydrobromic acid was heated at 80 °C and stirred using a magnetic stirrer for 20 minutes. The slow evaporation of the final solution at RT during two weeks yielded yellow platelets crystals of $(C_6H_7NBr)_3[CdBr_5]$, suitable for structure determination using X-ray diffraction in high yield (75%). The optical microscope image in Fig. 1(a) shows the morphology of the crystals.

X-ray crystallographic study

Single-crystal X-ray diffraction (XRD) data were collected using an APEX II, Bruker-AXS diffractometer with the Mo Kα radiation (λ = 0.71073 Å) at RT (293 K). The structure was solved with direct method and refined by full-matrix least-squares method based on F^2 using the SHELXT software.[42] The organic parts were found by the utilization of a successive Fourier calculation using the same software. All hydrogen atoms bonded to C and N atoms were geometrically assigned with a distance C–H = 0.97 Å and N–H = 0.89 Å. The crystallographic data and structure refinement conditions of $(C_6H_7NBr)_3[CdBr_5]$ are summarized in Table 1.

Thermal and vibrational studies

The thermal analyses of $(C_6H_7NBr)_3[CdBr_5]$ were performed on raw powders with a TGA/DTA 'SETSYS Evolution' (Pt crucibles,

Table 1 Crystal data and structure for 4-BAPC

Crystal data	
Chemical formula	$(C_6H_7NBr)_3[CdBr_5]$
M_r	1031.06
Crystal system, space group	Monoclinic, $P2_1/c$
Temperature (K)	293
a, b, c (Å)	15.4709 (14), 8.1826 (10), 23.466 (4)
β (°)	99.59 (1)
V (A^3)	2929.1 (7)
Z	4
Radiation type	Mo Kα radiation, $\lambda = 0.71073$ Å
μ (mm^{-1})	11.67 mm^{-1}
Crystal size (mm)	0.23 × 0.13 × 0.10
Data collection	
Diffractometer	APEXII, Bruker-AXS
Absorption correction	Multi-scan
T_{min}, T_{max}	0.170, 0.353
No. of measured, independent and observed [$I > 2\sigma(I)$]reflections	64 272, 6738, 4209
R_{int}	0.087
θ_{max}, θ_{min} (°)	27.5, 2.0
Refinement	
$R[F^2 > 2\sigma(F^2)]$, w$R(F^2)$, S	0.036, 0.091, 1.10
No. of reflections	6738
No. of parameters	274
No. of restraints	0
H-Atom treatment	H-Atom parameters constrained
$\Delta\rho_{max}$, $\Delta\rho_{min}$ (e Å^{-3})	0.68, −1.14

Al_2O_3 as a reference) under N_2 flow (100 ml min^{-1}). The thermograms were collected on 11.5 mg of the samples in a maximum temperature of 600 °C (heating speed of 5 °C min^{-1}).

The IR spectrum was recorded in the frequency range 4000–450 cm^{-1} at room temperature using a PerkinElmer FT-IR 1000 spectrometer. Sample was prepared as pellets with KBr as a dispersant.

Optical and photoluminescence measurements

The UV-vis diffuse reflectance spectrum of the 4-BAPC was performed at room temperature using a Varian Cary 5000 UV-vis-NIR spectrophotometer in the wavelength range between 200 and 800 nm. The PL spectra were collected using a Horiba FluoroMax 4 spectrometer at room temperature under different excitation wavelengths.

Calculation method

Density functional theory (DFT) calculation was conducted using the QUANTUM ESPRESSO package.[43,44] The generalized gradient approximation (GGA) as proposed by Perdew–Burke–Ernzerhof[45] was employed with projector-augmented wave (PAW) pseudopotentials with cutoff energies of 70 Ry for the plane-wave basis set and 420 Ry for the charge density. The Brillouin zone was sampled with a 3 × 6 × 2 Monkhorst–Pack mesh for structural optimization and self-consistent calculation. A structural relaxation was conducted for the atomic positions with a force on each atom smaller than 0.01 eV Å^{-1} and a convergence threshold on total energy for ionic minimization less than 10^{-6} Ry. The energy convergence for each self-consistency step was 10^{-6} Ry. A Gaussian smearing of 0.01 Ry was used.

$$w = 1/[\sigma^2 F_0{}^2 + (0.0247P)2 + 4.8948P]$$

where $P = (F_0{}^2 + 2F_c{}^2)/3$.

Results and discussion

Structure description

The single-crystal XRD analyses show that the 4-bromoanilinium tetrabromocadmate crystallizes in the monoclinic system with the centrosymmetric space group $P2_1/c$. All the cell parameters are listed in Table S1.† The asymmetric unit is formed of three 4-bromoanilinium cations $(C_6H_7NBr)^+$ and one pyramidal square based $[CdBr_5]^{3-}$ anion (Fig. 1(a)). The Cd atoms are octahedrally coordinated by six Br atoms, the length of the Cd–Br bonds vary between 2.729(8) and 2.98(7) Å and the Br–Cd–Br angles are ranging from 81.36(2)° to 173.44(2)° as shown in Table S1.† The inorganic framework is constituted by infinite helical chains, formed with corner chairing $CdBr_6$ octahedra, extending along b-axis, with the presence of two bridging and four terminal bromide atoms (Fig. 1(b)) similar to 1D perovskite-type structures such as $(NAEP)_2Pb_2Cl_{10}$ H_2O[39] and $[NH_3(CH_2)_2Br]_3CdBr_5$.[46]

Fig. S1† shows that the packing diagram is constituted by infinite corner-sharing chains linked to the organic cations by N–H···Br hydrogen bonds. The organic cations are symmetrically different, resulting in the existence of two different types of N–H···Br hydrogen bonds. The first type, shown in Fig. S1(b),† is generated by two organic cations with the nitrogen atoms N_2 and N_3 connected directly to the inorganic chains and occurred between two terminal bromide atoms of the same octahedra and one birding bromide atom of another octahedron from the same chain (N–H···Br distance equal to 2.678 Å). The second type of hydrogen bonds (Fig. S1(c)†) connects the inorganic chains to each other and it is generated by the third cation with nitrogen atom N1 between two adjacent octahedrons from two different chains by their terminal bromide atoms (N–H···Br distance equals to 2.570 Å). The difference in distances between the two hydrogen bond types probably implies that the shorter is slightly stronger. The hydrogen bond parameters are listed in Table S2.†

On the other hand, the analysis of the organic molecules Hirshfeld surfaces shows that they are connected together *via* C···Br (Fig. S2†) and C···H (Fig. S3†) short contacts. The existence of red spots on the surfaces of the organic rings mapped with shape index reveals the existence of Br···π and C–H···π interactions between the different organic moieties.

To determine the degree of the structure distortion we opt to define the parameter Δd, which indicate the deviations of the lengths of the Cd–Br distances within the $CdBr_6$ octahedra.

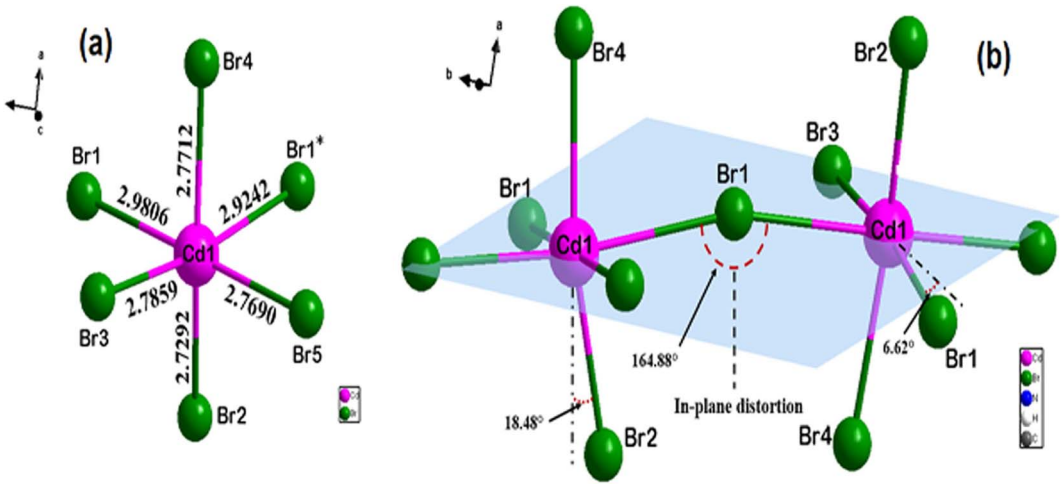

Fig. 2 Geometric description of the inorganic framework: (a) distorted $CdBr_6$ octahedron with different Cd–Br bond lengths and (b) distortion in adjacent octahedra.

$$\Delta d = \frac{1}{6}\sum_{n=1}^{6}\left(\frac{d_n - d}{d}\right)^2$$

where d is the average Cd–Br bond length (2.8266 Å) and d_n refers to the individual Cd–Br bonds in the octahedra. While the calculated Δd gives a value of 1.059×10^{-3}, proving that $CdBr_6$ octahedron is highly distorted in comparison with other octahedron in perovskite structures such as (2cepiH)$CdCl_3$ ($\Delta d = 2.58 \times 10^{-4}$),[40] $(mpz)_2PbBr_{10}$ ($\Delta d = 4.5 \times 10^{-4}$),[37] and α-(DMEN)$PbBr_4$ ($\Delta d = 1.7 \times 10^{-3}$).[47] It should be noted that the formation of hydrogen bonds between the organic and inorganic groups is in agreement with the different degrees of distortion affecting the adjacent cadmium octahedra (Fig. 2(b)).

Vibrational and thermal analysis

IR spectrum. Fig. S4† presents the infrared spectrum of the studied perovskite. We note the presence of two principal bands appearing around 2926 and 3039 cm^{-1}, which are generally attributed to the classical stretching vibrations of N–H related to the NH^{3+} groups, confirming the protonation of the 4-bromoaniline molecules. The bands appearing between 2574 and 480 cm^{-1} are attributed to the aromatic C–C and C–H vibrational modes of the organic groups.

Thermal analysis

The TG curve (Fig. S5†) shows that the 4-BAPC is stable up to 190 °C. Above this temperature, a weight loss is detected around 368 °C. During this process, the 4-BAPC loses 50% of its initial weight. This loss is assigned to the degradation of two organic molecules and the volatilization of two bromide ions, in the form of $(C_6H_6BrN)\cdot HBr$. The theoretical weight loss is 49.05% of the total mass. By correlating the structure of this material with the results of the thermogravimetric analysis, we can conclude that the departure of two organic cations in the first step confirms the difference in the strength of the hydrogen bonds that ensure the cohesion between these organic groups and the inorganic part. Indeed, the two cations $(C_6H_7BrN)^+$ linked *via* hydrogen bonds to a single chain probably decompose at the first time, while the third cation of the remaining compound appears to be more stable due to its connection with two different chains, thus playing the role of a junction bridge between them.

Semiconducting properties

In order to predict the electronic properties of the 4-BAPC, the solid-state diffuse reflectance spectrum of the synthesized compound was collected at room temperature. The absorption spectrum (Fig. 3(a)), was obtained from the reflectance spectrum using the Kubelka–Munk (K–M) function:

$$F(R) = \frac{(1-R)^2}{2R} = \frac{K}{S}$$

where R is the reflectance, K is the K–M absorption coefficient, and S is the scattering coefficient.[48] The 4-BAPC presents an absorption peak in the ultraviolet region with a wavelength around 270 nm. As presented in Fig. 3(a) the optical absorbance spectrum shows an intense absorption peak around 4.24 eV (292 nm), which is attributed to the electronic transition from the valence to the conduction band.[28,49,50] The weak bands observed between 2.5 and 4 eV are probably assigned to the excitons confined into the $[CdBr_5]_\infty 3-$ chains and to the charge transfer between the organic and the inorganic species. The band gap energies of 4-BAPC can be estimated from the Tauc plots as a function of the photon energy (hν). This method is often used to estimate an optical band gap of a given semiconductor with parabolic bands at the Fermi energy level. By means of a slight fitting of direct and indirect Tauc plots (Fig. 3(b) and (c)), the direct and indirect band gap energies were found to be $E_g^{d} = 4.27$ eV and $E_g^{ind} = 3.93$ eV, respectively. The obtained energy gap values are reasonable and close to others values of hybrid organic–inorganic Cd-based compounds from literature, such as the ferroelectric perovskite (3-

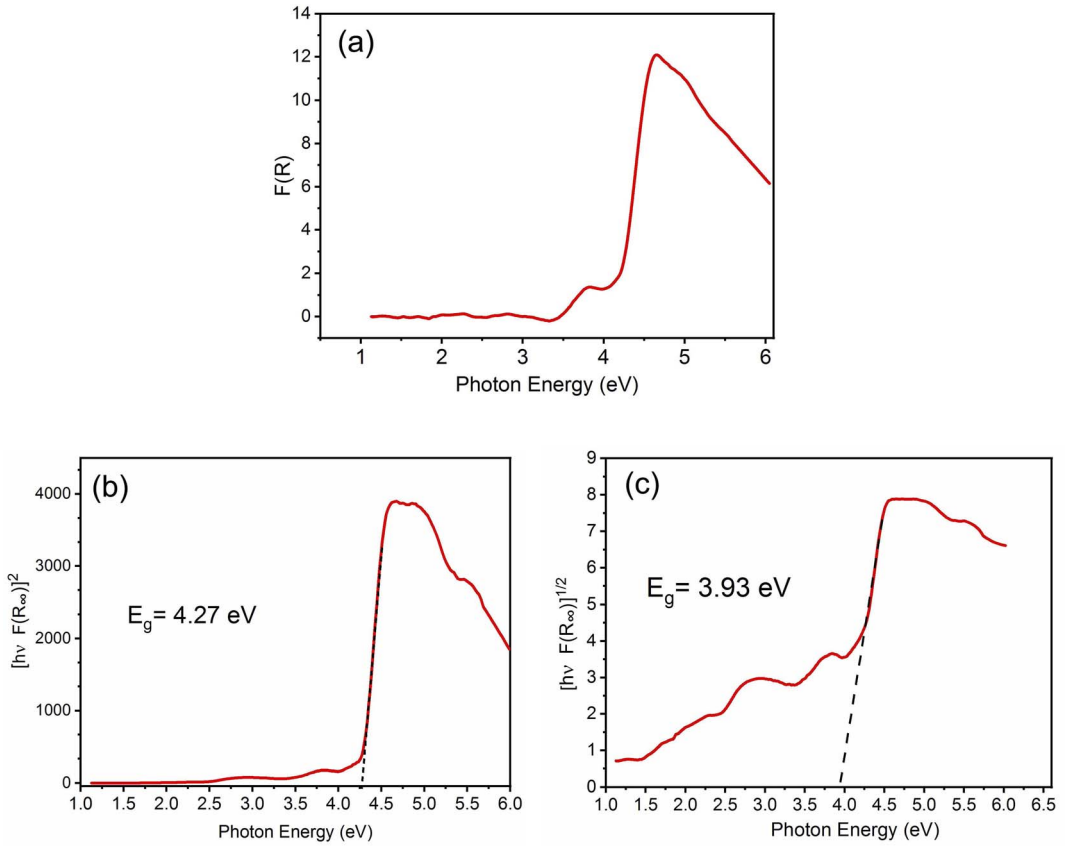

Fig. 3 (a) Kubelka–Munk absorption spectrum, (b) Tauc plot for direct gap and (c) Tauc plot for indirect gap (h is the Planck constant, ν is the vibrational frequency of the oscillator, and $F(R_\infty)$ is the K–M absorption coefficient).

pyrrolinium)$[CdCl_3]$[51] (4-5eV), the semiconductor $(C_5H_9NH_3)_4[CdBr_6]$ (4.58 eV), and $(C_5H_{12}N)[CdCl_3]$ (4.65 eV).[49,52]

To gain more insight into the electronic properties of this new perovskite, we have performed DFT calculations. Fig. 4(a) and (b) present the electronic band structure and the density of states (DOS), respectively. It is clear that our material has an indirect band gap of 3.16 eV, with the valence band maximum (VBM) located between C2 and Y2 points, and the conduction band minimum (CBM) at the Y2 valley of the Brillouin zone. The direct band gap located at Y2 point has a value close to that of the indirect band gap (only a few meV larger) as shown in Fig. S6 of the ESI.† The calculated band gap values are less than those measured optically (4.24 and 3.93 eV for the direct and indirect band gap, respectively), this is due to the fact that

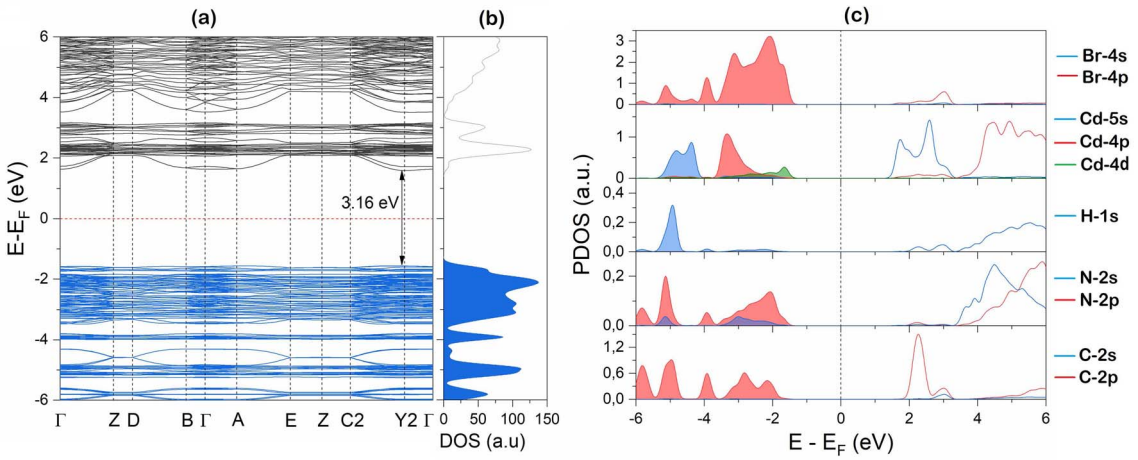

Fig. 4 DFT simulation of 4-BAPC (a) band structure, (b) total density of states (DOS), and (c) partial density of states (PDOS).

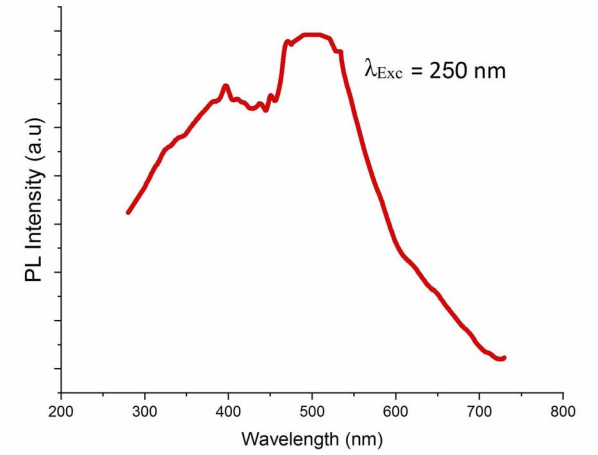

Fig. 5 PL spectrum of the (4-BAPC) under 250 nm.

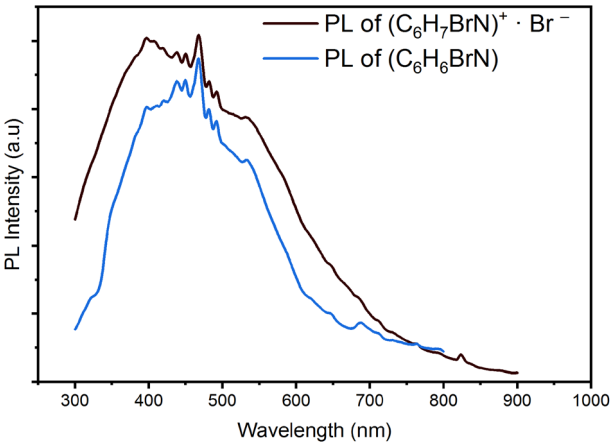

Fig. 7 PL spectra of the organic molecule C_6H_6BrN and $(C_6H_7BrN)^+ \cdot Br^-$ ammonium salt (λ_{Exc} = 200 nm).

the GGA method underestimates band gaps.[53] An analysis of the partial density of states (PDOS) displayed in Fig. 4(c), reveals that the VBM originates from a combination of Br-4p orbitals and Cd-4d orbitals, whereas the CBM originates from the Cd-5s orbital.

Photoluminescence

The photoluminescence of 4-BAPC was explored to investigate the photo-physical properties. Here, the material was excited under different energies to study its photoluminescent properties. It is well known that the sub-gap excitation ($E_{Exc} < E_g$) of Cd-based materials improves the self-trapping mechanism within the $CdBr_x$ clusters, and generates furthermore to the narrow excitonic emission, a broad-band covering the visible region leading to white light emission.[54,55] Hence, we use in this section two different excitation energies; the first one is above the gap value and the second one is below the gap value in order to enhance the emission through STE mechanism. In our case, the excitation of the material with photon energy higher than the band-gap, of 4.92 eV (250 nm), shows that the synthesized compound exhibits broad emission in the UV-vis region at room temperature (Fig. 5).

Under sub-gap excitation of 380 nm, the PL spectrum (Fig. 6(a)) shows that the 4-BAPC exhibits a wide emission band spanning the majority of the visible range. The main emission spectrum is similar to that observed in 1D and 0D Cd-based hybrid materials, such as $(2cepiH)CdCl_3$ (2cepi = 1-(2-chloroethyl)piperidine),[40] $(C_5H_9–NH_3)_4CdBr_6$,[49] and $(HMEDA)CdBr_4$ (HMEDA = hexamethylenediamine).[50] Fig. 6(b) shows the map of the chromaticity coordinates (x,y) of the emitted light in the CIE 1931 chromaticity diagram. The chromaticity coordinates of the light rays emitted by our material under 380 nm are (0.30, 0.32), very close to that of the ideal sun light (0.33, 0.33). The corresponding calculated CRI and CCT are 98 and 6812 K, respectively, indicating that the synthesized compound emit a cold white light with an extra high CRI.

Recently, several research papers proved the pertinent role of the π-conjugated organic cations in the emissive behaviors of hybrid materials. Depending on the molecular packing mode, the emission from organic cations can be phosphorescence or fluorescence in nature and then, the photoluminescence performances of hybrid materials can be tailored by modifying supramolecular assembly modes.[56] Hence, to scrutinize the emission origin within the 4-BAPC structure and to more

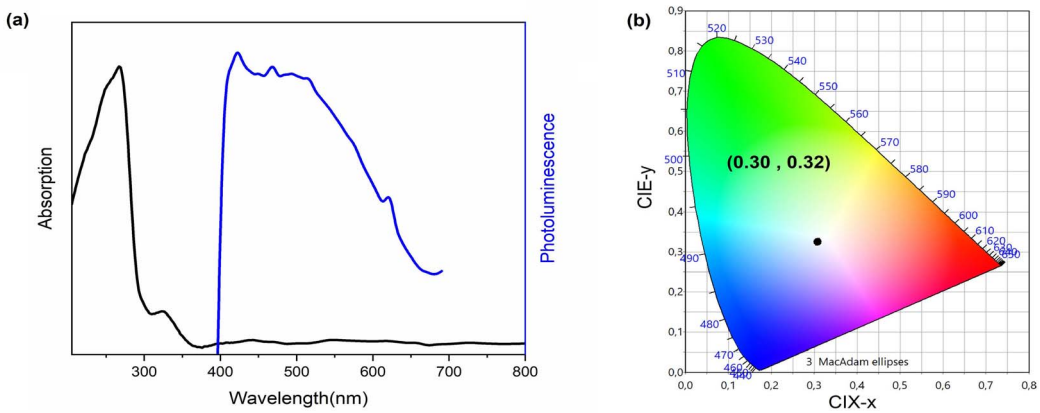

Fig. 6 (a) Absorption and emission spectra (λ_{exc} = 380 nm) of 4-BAPC and (b) CIE coordinates of the same compound.

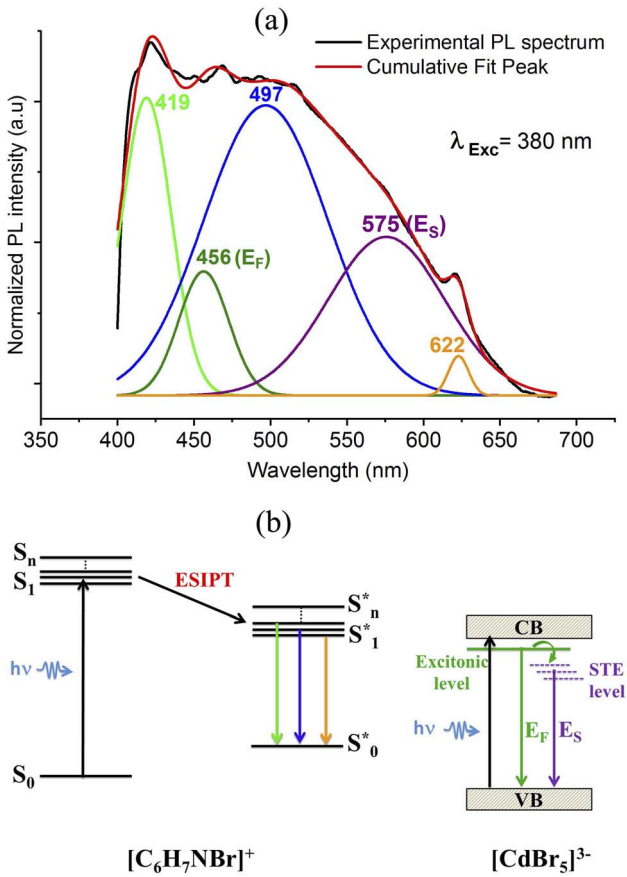

Fig. 8 Multi-peaks fitting of the PL spectrum of 4-BAPC (a) with the proposed emission diagram under subgap excitation of 380 nm (b).

understand the effect of the organic species $(C_6H_7BrN)^+$ on the photoluminescence properties, we recorded the emission spectra of the pure organic 4-bromoaniline (C_6H_6BrN) and the $(C_6H_7BrN)^+\cdot Br^-$ salt under excitation wavelength of 200 nm (Fig. 7). The emission spectra illustrate that they display an intense broad-band emission spanning the whole UV-vis region. The revealing of the white light emission from C_6H_6BrN and $(C_6H_7BrN)^+\cdot Br^-$ proves the emissive properties of the organic moieties.

In fact, recent researches on organic fluorescent materials show that intermolecular non-covalent interactions, such as anion$\cdots\pi$, C–H$\cdots\pi$ and N–H$\cdots\pi$, enhance the excited state intramolecular proton transfer (ESIPT) mechanism leading to an ultrafast fluorescence resulting from the transitions from different excited singlet states S_n^* to the excited states S_0^*.[57–59] On the other hand, $Br^-\cdots H^+$ hydrogen interactions can inhibit the molecular vibrational movement which improves the luminescence properties.[60] As shown in the structure description section, the XRD results demonstrate the existence of C–H$\cdots\pi$ and Br$\cdots\pi$ interactions between the different organic molecules (see Fig. S2 and S3†). As the structure of the pure organic molecule C_6H_6BrN was previously reported,[61] we analyse the Hirshfeld surface of the C_6H_6BrN molecule (Fig. S7†). This analysis shows that the organic molecules are linked through N–H$\cdots\pi$ and Br$\cdots\pi$ interactions. Hence, the fluorescence from

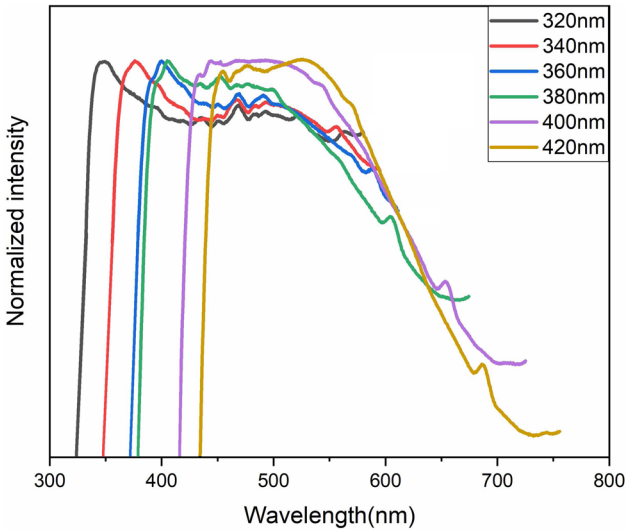

Fig. 9 Emission spectra of 4-BAPC with different wavelengths excitation at room temperature.

the pure organic C_6H_6BrN is stabilized through the ESIPT mechanism which remain observed within the 4-BAPC structure, where the N–H$\cdots\pi$ contacts were replaced by the C–H$\cdots\pi$ ones. Therefore, the emission of the white light from our material is due to the organic fluorescence and the STE within the inorganic sub-lattice.

To analyze the emission processes inside the crystal, a Gaussian deconvolution of the luminescence spectrum of the salt was realized (Fig. S8†). The best multi-peak fitting of the PL spectrum shows that the white light emission of the salt results from four overlapped fluorescence bands observed at 311, 383, 497 and 623 nm which originate from multi-excitonic transitions from excited singlet states S_n^* to the excited singlet state S_0^*. The comparison between the photoluminescence spectra of the $(C_6H_7BrN)^+\cdot Br^-$ salt (Fig. S8†) and that of $(C_6H_7NBr)_3[CdBr_5]$, Fig. 8(a), shows that the luminescence bands observed for the salt are also observed in the emission spectrum of the hybrid material. The appearance of two extra bands "E_F" at 456 and

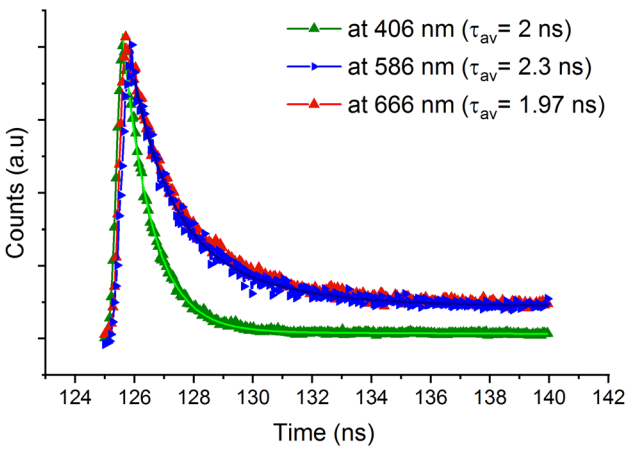

Fig. 10 The time resolved PL decays recorded under 365 nm.

"E_S" at 575 nm results from the free exciton's emission and the self-trapped exciton's emission within the inorganic cluster, respectively. The proposed PL mechanism within 4-BAPC is presented in Fig. 8(b). To study the effect the variation of the excitation energy on the luminescence properties of the material, the PL response of 4-BAPC was recorded under different excitation energies. As shown in Fig. 9, increasing the excitation energy from 320 to 420 nm, the broad band WLE from the material still observed.

The lifetime measurements were recorded and presented in Fig. 10. The time resolved PL decay of three emission peaks were recorded under excitation wavelength of 365 nm. The measured average lifetimes at 406, 586 and 666 nm were obtained by fitting the experimental data using a bi-exponential decay function and they are found to be 2, 1.97 and 2.3 ns, respectively. The fast decay of the emission bands confirms the fluorescence nature of 4-BAPC.

Conclusion

In summary, we report a new lead-free hybrid organic–inorganic perovskite-type, 4-BAPC, with 1D chains formed with corner-sharing $CdBr_6$ octahedra. The UV-vis absorption analysis shows that the 4-BAPC presents a large band gap energy which makes it suitable for optoelectronic applications. The calculated band structure reveals that the valence band originates from a combination of Br-4p orbitals and Cd-4d orbitals, whereas the conduction band originates from the Cd-5s orbital. The synthesized molecular crystal exhibit an efficient white-light emission characterized by an ultra-high CRI up to 98 and a CIE chromaticity coordinates of (0.30, 0.32) with a CCT of 6812 K. This emission results from the excitonic transition within the inorganic framework and from the fluorescence of the organic molecules.

Conflicts of interest

There are no conflicts to declare.

Acknowledgements

The authors extend their appreciation to the Deanship of Scientific Research at Imam Mohammad Ibn Saud Islamic University (IMSIU) for funding and supporting this work through Research Partnership Program no RP-21-09-71.

References

1 Y. L. Chang and Z. H. Lu, *J. Disp. Technol.*, 2013, **9**, 459–468.
2 T. H. Kim, W. Wang and Q. Li, *Front. Chem. Sci. Eng.*, 2012, **6**, 13–26.
3 S. W. Sanderson and K. L. Simons, *Resour. Policy*, 2014, **43**, 1730–1746.
4 I. Speier and M. Salsbury, *Sixth Int. Conf. Solid State Light.*, 2006, **6337**, 63371F.
5 Y. Ohno, *Fourth Int. Conf. Solid State Light.*, 2004, **5530**, 88.
6 S. Muthu and J. Gaines, *Conf. Rec. - IAS Annu. Meet.*, 2003, **1**, 515–522.
7 S. Muthu, F. J. P. Schuurmans and M. D. Pashley, *IEEE J. Sel. Top. Quantum Electron.*, 2002, **8**, 333–338.
8 K. H. Lee and S. W. R. Lee, *Proc. Electron. Packag. Technol. Conf., 4th*, 2006, 379–384.
9 J. Yum, S.-Y. Seo, S. Lee and Y.-E. Sung, *J. Electrochem. Soc.*, 2003, **150**, H47.
10 M. Pan, B. Bin Du, Y. X. Zhu, M. Q. Yue, Z. W. Wei and C. Y. Su, *Chem.–Eur. J.*, 2016, **22**, 2440–2451.
11 D. Chen, Z. Wan, Y. Zhou, X. Zhou, Y. Yu, J. Zhong, M. Ding and Z. Ji, *ACS Appl. Mater. Interfaces*, 2015, **7**, 19484–19493.
12 S. Ye, F. Xiao, Y. X. Pan, Y. Y. Ma and Q. Y. Zhang, *Mater. Sci. Eng., R*, 2010, **71**, 1–34.
13 D. B. Mitzi, S. Wang, C. A. Feild, C. A. Chess and A. M. Guloy, *Science*, 1995, **267**, 1473–1476.
14 R. J. Stead, M. A. Barradas, D. P. Mikhailidis, M. E. Hodson, J. C. Batten and P. Dandona, *Platelet function in patients with cystic fibrosis*, 1986, vol. 25.
15 D. B. Mitzi, C. A. Feild, Z. Schlesinger and R. B. Laibowitz, *J. Solid State Chem.*, 1995, 159–163.
16 D. B. Mitzi, C. A. Feild, W. T. A. Harrison and A. M. Guloy, *Nature*, 1994, **369**, 467–469.
17 K. A., T. K., S. Y. and M. T., *J. Am. Chem. Soc.*, 2009, **131**, 6050–6051.
18 M. Yuan, L. N. Quan, R. Comin, G. Walters, R. Sabatini, O. Voznyy, S. Hoogland, Y. Zhao, E. M. Beauregard, P. Kanjanaboos, Z. Lu, D. H. Kim and E. H. Sargent, *Nat. Nanotechnol.*, 2016, **11**, 872–877.
19 G. Li, Z. K. Tan, D. Di, M. L. Lai, L. Jiang, J. H. W. Lim, R. H. Friend and N. C. Greenham, *Nano Lett.*, 2015, **15**, 2640–2644.
20 H. Cho, S. H. Jeong, M. H. Park, Y. H. Kim, C. Wolf, C. L. Lee, J. H. Heo, A. Sadhanala, N. S. Myoung, S. Yoo, S. H. Im, R. H. Friend and T. W. Lee, *Science*, 2015, **350**, 1222–1225.
21 G. Xing, N. Mathews, S. S. Lim, N. Yantara, X. Liu, D. Sabba, M. Grätzel, S. Mhaisalkar and T. C. Sum, *Nat. Mater.*, 2014, **13**, 476–480.
22 F. X. Liang, L. Liang, X. Y. Zhao, L. B. Luo, Y. H. Liu, X. W. Tong, Z. X. Zhang and J. C. A. Huang, *Adv. Opt. Mater.*, 2019, **7**, 1–9.
23 E. R. Dohner, A. Jaffe, L. R. Bradshaw and H. I. Karunadasa, *J. Am. Chem. Soc.*, 2014, **136**, 13154–13157.
24 E. R. Dohner, E. T. Hoke and H. I. Karunadasa, *J. Am. Chem. Soc.*, 2014, **136**, 1718–1721.
25 A. Yangui, D. Garrot, J. S. Lauret, A. Lusson, G. Bouchez, E. Deleporte, S. Pillet, E. E. Bendeif, M. Castro, S. Triki, Y. Abid and K. Boukheddaden, *J. Phys. Chem. C*, 2015, **119**, 23638–23647.
26 R. Msalmi, S. Elleuch, B. Hamdi, E. Radicchi, A. Tozri, H. Naïli and M. R. Berber, *New J. Chem.*, 2021, **45**, 20850–20859.
27 K. Thirumal, W. K. Chong, W. Xie, R. Ganguly, S. K. Muduli, M. Sherburne, M. Asta, S. Mhaisalkar, T. C. Sum, H. Sen Soo and N. Mathews, *Chem. Mater.*, 2017, **29**, 3947–3953.
28 A. Yangui, S. Pillet, E. E. Bendeif, A. Lusson, S. Triki, Y. Abid and K. Boukheddaden, *ACS Photonics*, 2018, **5**, 1599–1611.

29 Y.-J. Tung, M. M. Lu, M. S. Weaver, M. Hack and J. J. Brown, *Org. Light. Mater. Devices VII*, 2004, **5214**, 114.
30 Q. Dai, C. E. Duty and M. Z. Hu, *Small*, 2010, **6**, 1577–1588.
31 J. J. Zhang, R. Hu, X. J. Yu, B. Xie and X. B. Luo, *Opt. Laser Technol.*, 2017, **88**, 161–165.
32 N. Sandor and H. Yaguchi, *Color Res. Appl.*, 2004, **29**, 168.
33 M. S. Rea and J. P. Freyssinier, *Color Res. Appl.*, 2010, **35**, 401–409.
34 G. He, J. Xu and H. Yan, *AIP Adv.*, 2011, **1**, 032160.
35 Y. Peng, Y. Yao, L. Li, Z. Wu, S. Wang and J. Luo, *J. Mater. Chem. C*, 2018, **6**, 6033–6037.
36 H. Barkaoui, H. Abid, S. Zelewski, J. Urban, M. Baranowski, A. Mlayah, S. Triki, P. Plochocka and Y. Abid, *Adv. Opt. Mater.*, 2019, **7**, 1–9.
37 L. Mao, P. Guo, M. Kepenekian, I. Hadar, C. Katan, J. Even, R. D. Schaller, C. C. Stoumpos and M. G. Kanatzidis, *J. Am. Chem. Soc.*, 2018, **140**, 13078–13088.
38 W. F. Zhang, W. J. Pan, T. Xu, R. Y. Song, Y. Y. Zhao, C. Y. Yue and X. W. Lei, *Inorg. Chem.*, 2020, **59**, 14085–14092.
39 D. Li, W. Wu, S. Wang, X. Zhang, L. Li, Y. Yao, Y. Peng and J. Luo, *J. Mater. Chem. C*, 2020, **8**, 6710–6714.
40 Z. Qi, Y. Chen, Y. Guo, X. Yang, F. Q. Zhang, G. Zhou and X. M. Zhang, *J. Mater. Chem. C*, 2021, **9**, 88–94.
41 D. Cortecchia, J. Yin, A. Petrozza and C. Soci, *Mater. Chem. C*, DOI: **10.1039/C9TC01036J**.
42 G. Sheldrick, *Acta Crystallogr.*, 2015, **71**, 3–8.
43 J. Enkovaara, C. Rostgaard and J. J. Mortensen, *Phys. Condens. Matter*, 2017, **29**, 465901.
44 P. Giannozzi, S. Baroni, N. Bonini, M. Calandra, R. Car, C. Cavazzoni, D. Ceresoli, G. L. Chiarotti, M. Cococcioni, I. Dabo, A. Dal Corso, S. De Gironcoli, S. Fabris, G. Fratesi, R. Gebauer, U. Gerstmann, C. Gougoussis, A. Kokalj, M. Lazzeri, L. Martin-Samos, N. Marzari, F. Mauri, R. Mazzarello, S. Paolini, A. Pasquarello, L. Paulatto, C. Sbraccia, S. Scandolo, G. Sclauzero, A. P. Seitsonen, A. Smogunov, P. Umari and R. M. Wentzcovitch, *J. Phys.: Condens. Matter*, 2009, **21**, 395502.
45 J. P. Perdew, K. Burke and M. Ernzerhof, *Phys. Rev. Lett.*, 1996, **77**, 3865–3868.
46 H. P. Chen, Z. X. Wang, C. Chen, Y. Lu, Z. Yin, X. F. Sun and D. W. Fu, *Dalton Trans.*, 2017, **46**, 4711–4716.
47 M. Lingling, W. Yilei, S. Constantinos C, R. W. Michael and G. K. Mercouri, *J. Am. Chem. Soc.*, 2017, **139**, 5210–5215.
48 G. Kortüm, W. Braun and G. Herzog, *Angew. Chem.*, 1963, **75**, 653–661.
49 W. Sasa, L. Li, Z. Sun, C. Ji, S. Liu, Z. Wu, S. Zhao, M. Hong and J. Luo, *J. Mater. Chem. C*, 2017, **5**, 4731–4735.
50 X. W. Sun, C. He, W. L. Liu, M. J. Pan, W. J. Dong, L. F. Chen and G. Lei, *Chem.–Asian J.*, 2020, **15**, 3050–3058.
51 M. Ferroelectricity, H. Ye, Y. Zhang and R. Xiong, *Angew. Chem., Int. Ed.*, 2014, **1–7**.
52 E. C. C. Baly, *Annu. Rep. Prog. Chem.*, 1913, **10**, 28–53.
53 L. Sun, W. Zhou, Y. Liang, L. Liu and P. Wu, *Comput. Mater. Sci.*, 2016, **117**, 489–495.
54 R. Msalmi, S. Elleuch, B. Hamdi, W. Abd El-Fattah, N. Ben Hamadi and H. Naili, *RSC Adv.*, 2022, **12**, 10431.
55 R. Roccanova, M. Houck, A. Yangui, D. Han, H. Shi, Y. Wu, D. T. Glatzhofer, D. R. Powell, S. Chen, H. Fourati, A. Lusson, K. Boukheddaden, M. Du and B. Saparov, *ACS Omega*, 2018, **3**, 18791–18802.
56 Z. Huang and X. Ma, *Cell Rep. Phys. Sci.*, 2020, **1**, 100167.
57 V. S. Padalkar and S. Seki, *Chem. Soc. Rev.*, 2016, **45**, 169–202.
58 A. Shahraki, A. Ebrahimi, S. Rezazadeh and R. Behazin, *Mol. Syst. Des. Eng.*, 2021, **6**, 66–79.
59 H. C. Joshi and L. Antonov, *Molecules*, 2021, **26**, 1475.
60 S. Feng, Q. Huang, S. Yang, Z. Lin and Q. Ling, *Chem. Sci.*, 2021, 14451–14458.
61 A. Dey, R. K. R. Jetti, R. Boese and G. R. Desiraju, *CrystEngComm*, 2003, **5**, 248–252.